From CMIP3 to CMIP6: Northern Hemisphere Atmospheric Blocking Simulation in Present and Future Climate

Paolo Davini, Fabio d'Andrea

From CMIP3 to CMIP6: Northern Hemisphere Atmospheric Blocking Simulation in Present and Future Climate

PAOLO DAVINI

Istituto di Scienze dell'Atmosfera e del Clima, Consiglio Nazionale delle Ricerche (CNR-ISAC), Torino, Italy

FABIO D'ANDREA

Laboratoire de Météorologie Dynamique/IPSL, École Normale Supérieure, PSL Research University, CNRS, Paris, France

(Manuscript received 18 November 2019, in final form 13 July 2020)

ABSTRACT

A comprehensive analysis of the representation of winter and summer Northern Hemisphere atmospheric blocking in global climate simulations in both present and future climate is presented. Three generations of climate models are considered: CMIP3 (2007), CMIP5 (2012), and CMIP6 (2019). All models show common and extended underestimation of blocking frequencies, but a reduction of the negative biases in successive model generations is observed. However, in some specific regions and seasons such as the winter European sector, even CMIP6 models are not yet able to achieve the observed blocking frequency. For future decades the vast majority of models simulate a decrease of blocking frequency in both winter and summer, with the exception of summer blocking over the Urals and winter blocking over western North America. Winter predicted decreases may be even larger than currently estimated considering that models with larger blocking frequencies, and hence generally smaller errors, show larger reduction. Nonetheless, trends computed over the historical period are weak and often contrast with observations: this is particularly worrisome for summer Greenland blocking where models and observations significantly disagree. Finally, the intensity of global warming is related to blocking changes: wintertime European and North Pacific blocking are expected to decrease following larger global mean temperatures, while Ural summer blocking is expected to increase.

KEYWORDS: Blocking; Jets; Climate change; Climate sensitivity; Climate models; Climate variability

1. Introduction

Midlatitude atmospheric blocking is one of the most studied weather patterns in current weather and climate science. It involves a large-scale quasi-stationary high pressure system that can persist for several days, blocking or diverting the usual path of synoptic disturbances (Rex 1950). Blocking has always been an issue for both weather prediction and climate models due to its peculiar nature, which is hard to be correctly numerically simulated (Tibaldi and Molteni 1990; D'Andrea et al. 1998). Several generations of climate models have been shown to have significant negative biases in blocking frequency, especially evident over the European sector (Scaife et al. 2010; Masato et al. 2013; Davini and D'Andrea 2016; Woollings et al. 2018; Schiemann et al. 2020).

The origin of such underestimation has been often connected with a wrong representation of the mean state that affects Rossby wave propagation. Benefits to blocking representation have been found to be provided by 1) increasing the atmospheric horizontal resolution (Jung et al. 2012; Davini and D'Andrea 2016; Schiemann et al. 2020), 2) reducing the North Atlantic sea surface temperature (SST) bias (Scaife et al. 2011), and 3) improving tropical convection (Jung et al. 2010; Gollan et al. 2019). There is an indication that the position of the Gulf Stream (O'Reilly et al. 2016) and the intensity of the orographic drag (Pithan et al. 2016) can

Denotes content that is immediately available upon publication as open access.

Supplemental information related to this paper is available at the Journals Online website: https://doi.org/10.1175/JCLI-D-19-0862.s1.

Corresponding author: P. Davini, p.davini@isac.cnr.it

DOI: 10.1175/JCLI-D-19-0862.1

affect the Euro-Atlantic blocking representation. Recently, diabatic processes in ascending air masses upstream of the block have been found to be important for blocking onset (Pfahl et al. 2015; Steinfeld and Pfahl 2019), although implications for numerical simulations are still under investigation (Steinfeld et al. 2020). Unfortunately, a solution to the atmospheric blocking biases problem does not seem to have a unique recipe: for instance, increased horizontal resolution can lead to contradictory results (Schiemann et al. 2017) and improvements can be due to compensation of errors (Davini et al. 2017).

Given the large biases that still affect blocking simulation, the estimation of their change in the future climate has always been a concern for climate modelers, especially considering the large impact that blocking has on regional weather (Sillmann et al. 2011; Schaller et al. 2018). The increase in extreme events characterized by large waviness and meridional heat transport as hypothesized in the recent years (e.g., Francis and Vavrus 2012; Overland et al. 2016) has brought further attention to the role of low-frequency anomalies, among which blocking is one of the best known. There is an overall consensus that blocking frequency should decrease in the next century (Dunn-Sigouin and Son 2013; Masato et al. 2013; Woollings et al. 2018) but this may be dependent on the blocking index used (Woollings et al. 2018). Moreover, the presence of any trend is hardly measurable in observations (Davini et al. 2012; Barnes et al. 2014).

A huge coordinated effort by the climate modeling community has produced phase 6 of the Coupled Model Intercomparison Project (CMIP6; Eyring et al. 2016) where state-of-the-art global climate models (GCMs) with finer resolution and improved parameterizations are run with a common setup. Given the similarities with the previous phase 3 (CMIP3; Meehl et al. 2007) and phase 5 (CMIP5; Taylor et al. 2012) we have the opportunity to investigate over a large time window the biases and projected changes of the current and past generations of GCMs.

The present work aims at assessing the winter and summer atmospheric blocking characteristics in the last three modeling intercomparison efforts, namely CMIP3, CMIP5, and CMIP6, in both historical and future scenarios. The focus will be on coupled GCMs or Earth system models, collecting more than 75 climate models.

The biases in blocking frequencies of the three generations of models will be presented (section 3) as well as their predicted changes for the last part of the twenty-first century (section 4). Special attention will be paid to blocking frequency trends and to changes in interannual variability, which could affect the frequency of associated extreme events. Finally, in section 5 we will try to reconcile the changes in blocking frequency to the intensity of global warming.

2. Data and method

We make use of three different intercomparison project datasets, the CMIP3 (Meehl et al. 2007), CMIP5 (Taylor et al. 2012), and CMIP6 (Eyring et al. 2016) datasets. For each coupled model available in each dataset a single ensemble member is selected (picking the lowest ensemble number available). The reference period is 1961–2000 for the historical simulations: this is the largest time window available for a complete intersection of the datasets. On this window 19 CMIP3 models, 28 CMIP5 models, and 31 CMIP6 models are freely downloadable from the Earth System Gateway Federation (ESGF) archives. The scenarios where the largest increase of greenhouse concentration is expected to occur—SRES-A2 for CMIP3 (Nakicenovic et al. 2000), RCP8.5 for CMIP5 (Moss et al. 2010), and SSP5–8.5 for CMIP6 (O'Neill et al. 2016)—are used to estimate the effect of climate change on blocking statistics. A slightly reduced set of models is then available: 13 CMIP3 models, 27 CMIP5 models, and 21 CMIP6 models. For such scenarios, the comparison is carried out over the 2061–2100 window (2081–2100 for CMIP3 since for this project the data are limited to this period). However, the entire datasets available are taken into consideration when estimating blocking time series and trends.

Both winter and summer are analyzed, considering the extended seasons from December to March (DJFM) and from June to September (JJAS). Multiple reanalysis datasets are chosen to assess the bias of climate models: specifically, JRA-55 (Kobayashi et al. 2015), the NCEP–NCAR reanalysis (Kalnay et al. 1996) and—in order to cover the presatellite era—a combined ECMWF reanalysis consisting of ERA-40 (Uppala et al. 2005) from 1958 to 1978 and ERA-Interim (Dee et al. 2011) from 1979 to 2017. The three datasets are averaged together and defined as OBS throughout the text.

Most relevant dataset features are reported in Table 1, while a complete list of the CMIP models is reported in in the online supplemental material in Table X1 (CMIP3), Table X2 (CMIP5), and Table X3 (CMIP6).

The choice of a blocking index is a necessary and fundamental step for this work, but it is also a potential and hardly avoidable limitation. By and large, three main types of indices can be identified: 1) those based on the topology of the flow and defined observing gradients in geopotential or PV fields (e.g., Tibaldi and Molteni 1990; Pelly and Hoskins 2003) and 2) those based on anomalies with respect to a base state or a threshold

TABLE 1. Properties of the analyzed datasets. Resolution is estimated as the root square sum of the longitudinal and latitudinal resolutions; ΔT is the 2061–2100 minus 1961–2000 2-m temperature difference, zg is geopotential height, and ua is zonal wind.

Project (variable)	Experiment	Years	N models	Resolution (°)	ΔT (°C)
OBS (zg,ua)	NCEP–NCAR	1951–2017		2.5	
	JRA-55	1958–2017		0.55	
	ERA-40/ERA-Interim	1958–2017		1.15/0.70	
CMIP3 (ua)	Historical	1961–2000	19	4.04 ± 1.49	3.38 ± 0.39
	SRES-A2	2041–60, 2081–2100	13		
CMIP5 (zg)	Historical	1951–2005	28	2.84 ± 1.06	3.68 ± 0.56
	RCP-8.5	2006–2100	27		
CMIP6 (zg)	Historical	1951–2014	31	2.24 ± 0.83	4.14 ± 0.97
	SSP5–8.5	2015–2100	21		

(e.g., Dole and Gordon 1983; Schwierz et al. 2004), to which 3) a group of hybrid approaches can be added (e.g., Dunn-Sigouin and Son 2013). A review of the different blocking indices can be found in Barriopedro et al. (2010) and an extensive discussion on the difference resulting from the use of different indices has been given by several authors (Barnes et al. 2012; Woollings et al. 2018; Pinheiro et al. 2019).

Although all indices result in the main features of blocking climatology to agree, their variability and trends can have differences, depending on the season and on the region (Woollings et al. 2018). In this work the 2D blocking index based on the reversal of the geopotential height gradient at 500 hPa is used—belonging thus to the first of the above-mentioned categories. Our preference for a gradient-based index rather than an anomaly index is mainly motivated by the inherent difficulty caused by using an index based on anomalies for climate change scenarios. However, for the sake of completeness, the biases with an absolute index [based on a version similar to Schwierz et al. (2004)] are presented in the online supplemental material; see Fig. S3.

The index is the 2D extension from 30° to 75°N of the canonical definition by Tibaldi and Molteni (1990), as introduced by Scherrer et al. (2006). However, we here adopt a blocking definition that includes a third supplementary condition south of the blocked region aimed at excluding the low-latitude blocking events [see Davini et al. (2012) for details]. Defining Z500 as the daily geopotential height at 500 hPa interpolated on a common regular 2.5° × 2.5° grid, three meridional gradients are considered:

$$\mathrm{GHGS}(\lambda_0,\phi_0)=\frac{Z500(\lambda_0,\phi_0)-Z500(\lambda_0,\phi_\mathrm{S})}{\phi_0-\phi_\mathrm{S}}, \quad (1)$$

$$\mathrm{GHGN}(\lambda_0,\phi_0)=\frac{Z500(\lambda_0,\phi_\mathrm{N})-Z500(\lambda_0,\phi_0)}{\phi_\mathrm{N}-\phi_0}, \quad (2)$$

$$\mathrm{GHGS}_2(\lambda_0,\phi_0)=\frac{Z500(\lambda_0,\phi_\mathrm{S})-Z500(\lambda_0,\phi_{\mathrm{S}_2})}{\phi_\mathrm{S}-\phi_{\mathrm{S}_2}}, \quad (3)$$

and ϕ_0 ranges from 30° to 75°N while λ_0 ranges from 0° to 360°; $\phi_\mathrm{S}=\phi_0-15°$, $\phi_\mathrm{N}=\phi_0+15°$, and $\phi_{\mathrm{S}_2}=\phi_0-30°$. Instantaneous blocking is thus identified when

$$\mathrm{GHGS}(\lambda_0,\phi_0)>0, \quad \mathrm{GHGN}(\lambda_0,\phi_0)<-\frac{10\,\mathrm{m}}{°\mathrm{lat}},$$
$$\mathrm{GHGS}_2(\lambda_0,\phi_0)<-\frac{5\,\mathrm{m}}{°\mathrm{lat}} \quad (4)$$

so that a specific grid point is considered as blocked if all the three conditions above are satisfied simultaneously. Such conditions require an anomalous easterly flow in midlatitudes bounded by westerly flow to the north and to the south of the blocked grid point. Blocking is then measured as the percentage of blocked days per season.

We then avoid all temporal and spatial filtering to the instantaneous blocking definition. This is an unconventional decision for blocking analysis and it is a bit counterintuitive since blocking by definition requires a large spatial extent and a minimum duration (usually a 5-day minimum; Rex 1950). However, our choice relies on three main reasons:

- The results are not qualitatively different when the above mentioned filtering is applied [as by Davini et al. (2012)]. This can be seen by comparing Fig. 1 and Fig. S2.
- Given the large spread of blocking definitions a simpler blocking diagnostic of easy implementation and interpretation would be beneficial for future comparison.
- Previous works has already followed this approach (e.g., Tibaldi and Molteni 1990; Prodhomme et al. 2016).

The whole set of blocking data has been produced with the Mid-Latitude Evaluation System (MiLES) R

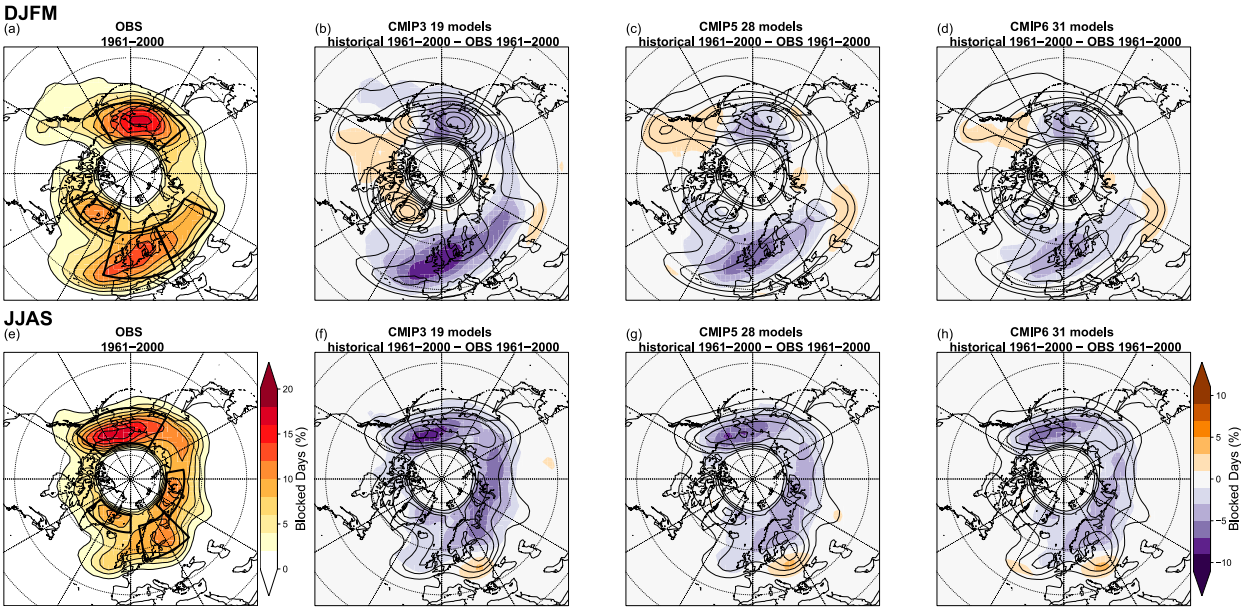

FIG. 1. (a),(e) 1961–2000 OBS blocking climatological frequency (contours and shading). Also shown is 1961–2000 MMM for blocking frequency (contours) and its bias against OBS (shading) for (b),(f) CMIP3, (c),(g) CMIP5, and (d),(h) CMIP6. Rows cover (top) winter (DJFM) and (bottom) summer (JJAS). Solid boxes in (a) and (e) identify the North Pacific, Greenland, central/eastern Europe, and Ural sectors. Contours are drawn every 2%.

suite (Davini 2019). This is a free tool available on GitHub that provides several blocking definitions and diagnostics.

Considering that CMIP3 models did not provide daily data for geopotential height, following Scaife et al. (2010) and Davini and D'Andrea (2016) the geostrophic approximation is used in order to estimate blocking frequencies from the eastward zonal wind at 500 hPa. This alternative blocking index, which mainly requires the presence of easterly winds in the midlatitudes, provides a reasonable blocking climatology that is characterized by a slight overestimation of blocking events on the order of 1%–2% of blocked days (see Fig. S1).

Considering this limitation, in the text atmospheric blocking frequencies are always reported as anomalies to the correspondent reference observational index. This implies that CMIP3 frequencies are shown as anomalies from the zonal wind index from OBS, while CMIP5 and CMIP6 are anomalies from the geopotential height index from OBS. When a single OBS value is reported this is always pointing to the value measured with the geopotential height index.

Moreover, in order to assess mean wind biases, monthly zonal wind at 500 hPa is taken into consideration for each model. Finally, in order to estimate the relation between global warming, atmospheric blocking, and surface temperature biases, monthly 2-m temperature are also examined.

3. Historical simulations

a. Mean bias

The atmospheric blocking climatologies for OBS are shown in Fig. 1. In the cold season (Fig. 1a), blocking shows the well-established maxima over central Europe, Greenland, and the North Pacific, with maximum frequencies found on the latter sector achieving about 20% of blocked days per season (Scherrer et al. 2006). Blocking over Greenland and North Pacific, characterized by cyclonic wave breaking, is often defined as high-latitude blocking since it is too far north to actually obstruct the flow and it tends to only divert the jet stream equatorward (Berrisford et al. 2007). Their impact on weather is however very relevant and Greenland blocking is tied with the North Atlantic Oscillation (Woollings et al. 2010). During summertime (Fig. 1e), the poleward shift of the jet pushes the preferred location for European blocking maximum over Finland. Although they are subject to an eastward displacement, the two maxima over Greenland and the North Pacific are still present. A secondary maximum develops also over western Russia and the Kara and Laptev Seas. This is the area known for the Ural blocking (Cheung et al. 2013; Luo et al. 2016). This region will be analyzed in the following sections along with the European, Greenland, and North Pacific sectors (see black boxes in Figs. 1a,e).

Differences between the multimodel mean (MMM) and observed blocking for the CMIP3, CMIP5, and

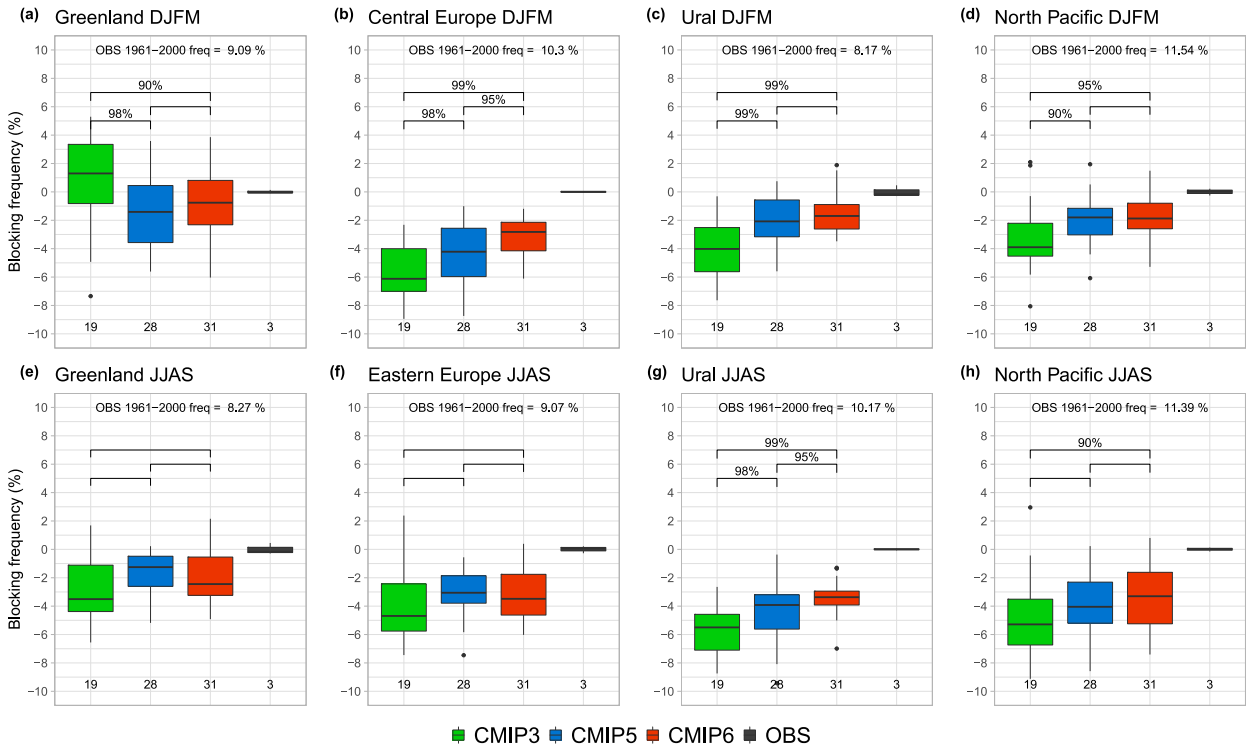

FIG. 2. 1961–2000 box plots for blocking frequency biases over the (a),(e) Greenland, (b),(f) central/eastern Europe, (c),(g) Ural, and (d),(h) North Pacific regions in (top) winter (DJFM) and (bottom) summer (JJAS). The lower, central, and upper lines show the first quartile, the median, and the third quartile, respectively. The upper (lower) whisker extends from the third (first) quartile to the largest (smallest) value in the ensemble, but limited to an upper bound that is 1.5 times the interquartile range (i.e. the distance between the third and first quartiles). Black dots show outliers from the whiskers. The number of models included in each bar is reported at the bottom. The observed blocking frequency (%, according to the geopotential height index) is shown at the top of each panel. The statistical significance (computed with a Welch *t* test) difference between CMIP ensembles pairs is reported above each boxplot.

CMIP6 are shown in the remaining panels of Fig. 1. In winter (Fig. 1, top row), all the CMIP families show the well-known negative bias over the central European region where a lack of anticyclonic wave breaking affects the simulated blocking frequencies. However, the bias seems considerably alleviated when moving from CMIP3 to CMIP6, going from about –7%/–8% (with climatological values around 10%/12%) up to –4%/–5%. A similar improvement is observed over the North Pacific, where the negative bias is substantially reduced in CMIP5 and CMIP6. However, some chronic misplacement of the blocking activity (usually extended toward the North American continent) is observed. Indeed, both the North Pacific and European biases are associated with the overestimation of the Pacific and Atlantic jet stream speeds and extensions (see Fig. S4), a common feature in several climate models (Anstey et al. 2013; Delcambre et al. 2013; Pithan et al. 2016). Conversely, the positive bias over Greenland found in CMIP3 models, likely associated with a wrong jet dynamics (Barnes and Hartmann 2010), becomes weakly negative in CMIP5 and CMIP6, suggesting a better representation of the North Atlantic Oscillation.

A similar negative bias is observed in summer (Fig. 1, bottom row). Indeed, all the MMMs show widespread underestimation of blocking activity almost everywhere in the Northern Hemisphere, with a negative bias over North Pacific, northern Europe, and the Urals. However, as seen in winter, such biases are reduced going from CMIP3 to CMIP5, becoming negligible over Greenland. Conversely to what is seen in winter, CMIP6 does not seem to carry any relevant improvement from CMIP5. It is interesting to observe the presence of a common and persistent positive bias over eastern Europe in all the intercomparison projects, showing an equatorward displacement of the summer European blocking activity.

The overall improvement occurred in the last 15 years can be better appreciated by looking at Fig. 2, where the boxplots for the averaged blocking frequencies over four specific sectors are reported. These sectors (shown by solid boxes in Figs. 1a and 1e) are slightly different between summer and winter in order to accommodate the shift of the blocking frequency maxima. For all the

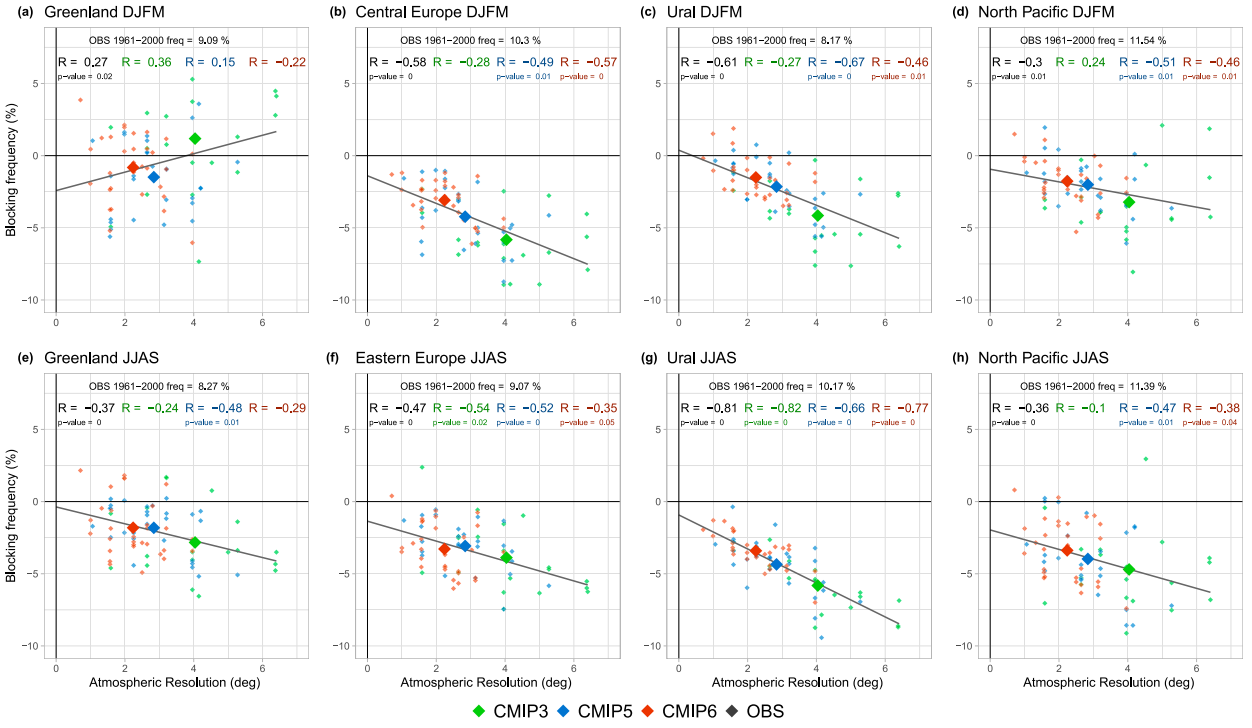

FIG. 3. Scatterplots between the horizontal resolution of each model and their bias in the historical period over the (a),(e) Greenland, (b),(f) central/eastern Europe, (c),(g) Ural, and (d),(h) North Pacific regions for (top) winter (DJFM) and (bottom) summer (JJAS). The gray line represents the linear fit among all the data. The Pearson correlation coefficients and their p values (only when the 10% significance with a t test is achieved) are shown at the top of each panel: black is for the complete CMIP dataset, and colors are used for the different intercomparison projects. The observed blocking frequency (%, according to the geopotential height index) is shown at the top of each panel.

regions and seasons an improvement in model performance with time is found. In synthesis, the biases have been halved from CMIP3 to CMIP6: for example, the MMM error decreased from −6% to −3% over winter central Europe, or from −4% to −2% over winter North Pacific. It should be noticed that climatological values of atmospheric blocking in these regions ranges between 9% and 11.5%, implying that CMIP6 errors are still about relatively 20%–30% of the OBS values. Better results have been obtained over Greenland, especially in winter. Here we can see how models, even if they are characterized by a large spread, are very close to OBS. At first order, this testifies the effort put by the climate modeling community to reduce bias in the simulation of the North Atlantic Oscillation (e.g., Dunstone et al. 2016).

However, a cautionary note on the improvement seen discussed so far should be added. Indeed, Fig. 2 shows also when the differences between each intercomparison project can be assumed as statistically significant. Results are largely positive for winter blocking, always showing robust improvement from CMIP3 to CMIP5 and for the European sector also from CMIP5 to CMIP6. Conversely the improvements are less evident in summer, where only the Ural sector shows a robust change. It is fair to conclude that even if the MMM values clearly show smaller biases for CMIP6 models, these are mostly significant only during wintertime.

b. *Horizontal resolution*

Since many works (e.g., Jung et al. 2012; Davini and D'Andrea 2016) pointed to the beneficial effect that horizontal resolution may have on atmospheric blocking representation, this has been investigated in Fig. 3. Here the atmospheric resolution of each model (expressed as the root square sum of the longitudinal and latitudinal resolutions) is plotted against the blocking bias in the four main regions in both winter and summer. A couple of indications emerge clearly: 1) in almost all sectors and in both seasons there is a reduction of the bias following resolution refinement (which is most robust over the European and the Ural sector, but significant everywhere) and 2) the linear fit across all the points rarely crosses the zero-bias line (and often stays below it), suggesting that further increases in horizontal resolution alone are unlikely to solve the current errors. The only

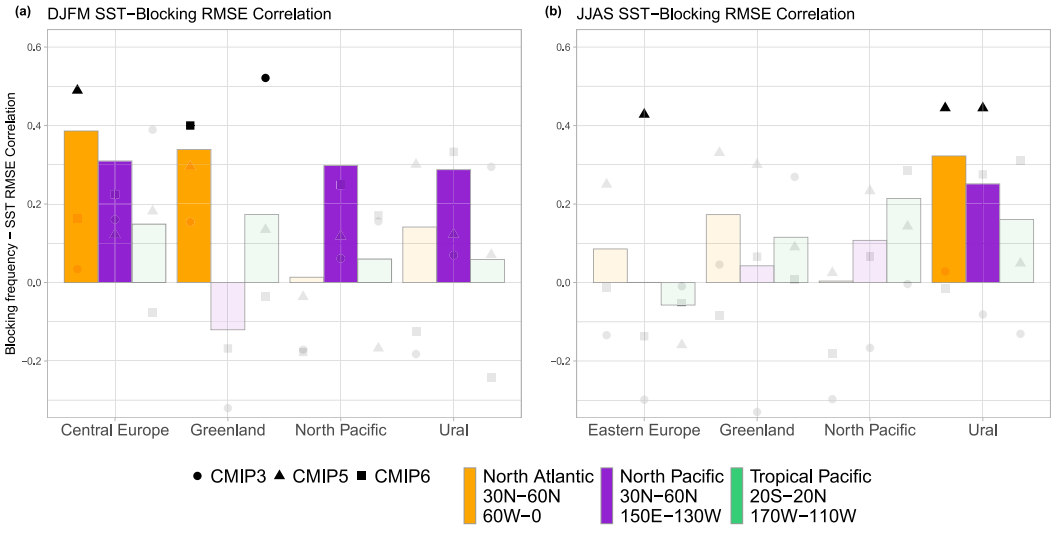

FIG. 4. (a) Winter and (b) summer Pearson correlation coefficients among atmospheric blocking RMSE (for the Greenland, central/eastern Europe, Ural, and North Pacific regions) and 2-m temperature RMSE (for three oceanic regions: the North Atlantic, North Pacific, and tropical Pacific). Bars shows the correlation over the entire CMIP datasets; circles, triangles, and squares indicate the correlation for CMIP3, CMIP5, and CMIP6, respectively. Transparency implies that values are not significant at the 5% level using a *t* test.

exception is winter Greenland blocking, where the bias is already small and the emerging correlation does not have a clear physical sense.

Of course, it should be kept in mind that—on average—recent models have finer horizontal resolution but also improved parameterizations than older models, so that it is impossible to disentangle the two effects on blocking frequencies. Anyway, considering that for most of the sectors (with Greenland being the only exception) the correlations are valid also when each intercomparison project is analyzed independently, it is possible to state that the emerging correlation between resolution and blocking bias is a robust feature in GCMs.

c. *Sea surface temperature*

Several works have pointed to a possible connection between sea surface temperature biases and the representation of atmospheric blocking (e.g., Scaife et al. 2011; O'Reilly et al. 2016). It has been also shown that a few selected atmosphere-only GCMs are able to reproduce European blocking almost correctly (Matsueda et al. 2009; Schiemann et al. 2017)—although sometimes following compensating errors (Davini et al. 2017)—suggesting a relevant role for atmosphere–ocean coupling in deteriorating model performance.

The role of SST biases is therefore explored by comparing the atmospheric blocking root-mean-square error (RMSE) over the four main regions with the 2-m surface temperature RMSE over selected oceanic regions, namely the North Atlantic (30°–70°N, 60°W–0°), the North Pacific (20°–60°N, 150°E–150°W), and the tropical Pacific (20°S–20°N, 170°–110°W). Eight models (CMIP3 GISS-AOM, IAP-FGOALS1.0-g, and MIROC3.2-hires; CMIP5 BNU-ESM and FGOALS-g2; CMIP6 GFDL-CM4, FGOALS-f3-L, and TaiESM1) have been excluded due to unavailability of historical 2-m temperature data. Figure 4 reports the Pearson correlation coefficients—in the model space—computed for each blocking and oceanic region.

Most of the correlation coefficients are positive, implying the expected reduction of the atmospheric blocking error for a smaller oceanic bias. Significance at the 5% level (with a *t* test) is attained only in a few instances: not surprisingly, winter European and Greenland blocking seems to be favored by an improved North Atlantic surface temperature [in agreement with Scaife et al. (2011)]. During summer the positive effects of an improved North Atlantic surface temperature are only seen over the Ural sector. While the tropical Pacific temperature bias seems to not have any relation with blocking simulation, North Pacific surface temperatures are surprisingly correlated with several blocking regions. Positive significant correlations are found for the European (in winter only) and Ural sectors and of course for the winter North Pacific too.

However, when inspecting each intercomparison project separately, the correlation coefficients often drop below the significance levels, with only CMIP5 showing multiple positive correlations. Given these findings—and that 1) a considerable sensitivity to the

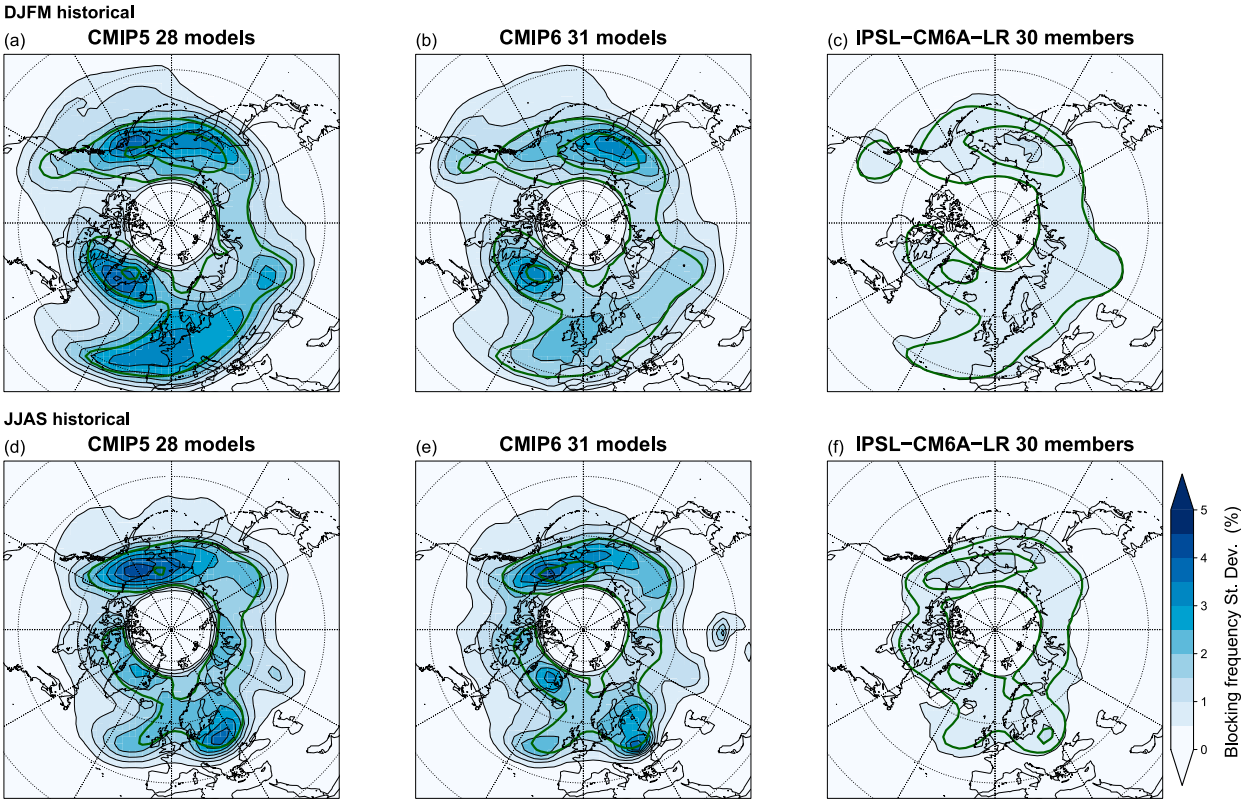

FIG. 5. Standard deviation of climatological blocking frequency for the historical period (1961–2000) across the (a),(d) CMIP5 ensemble, (b),(e) CMIP6 ensemble, and (c),(f) IPSL-CM6A-LR ensemble for (top) winter (DJFM) and (bottom) summer (JJAS). The MMM blocking frequency in the 1961–2000 historical simulation is shown in green contours (drawn every 5%).

oceanic region boundaries has been found (not shown) and 2) some of the significant correlations found are dynamically counterintuitive (e.g., Ural blocking and North Pacific surface temperature)—it is not possible to conclude that smaller oceanic temperature biases are associated with smaller blocking biases. Further work should be carried out in this direction, comparing atmosphere-only and coupled runs for each model separately (e.g., Davini and D'Andrea 2016) and considering possible stronger relationships that may exist over more specific oceanic subsectors (e.g., Hinton et al. 2009).

d. *Ensemble spread*

The large intermodel spread (which can be different from region to region) is already quite evident from Figs. 2 and 3. A more detailed look at this is given by Fig. 5, which shows the standard deviation from the 40-yr climatology of 28 CMIP5 models (Figs. 5a,d) and 31 CMIP6 models (Figs. 5b,e). CMIP3 has been excluded from this analysis considering that its results are based on the zonal wind blocking index. It is possible to see that there is larger agreement among CMIP6 models than in CMIP5, especially evident in winter. However, the intermodel spread remains quite large when compared to climatological values of blocking frequency.

In Figs. 5c and 5f the standard deviation from 30 members of the CMIP6 IPSL-CM6A-LR model is also shown: this is done in order to compare directly the intermodel spread (i.e., the spread among models from the same intercomparison project) to the intramodel spread (i.e., the spread among ensemble members of the same model). IPSL-CM6A-LR was chosen since it is the model providing the larger ensemble on the ESGF archives; however, similar results are obtained using smaller ensembles as CESM2 and CanESM5 (respectively, 10 and 25 members; not shown). The CMIP6 intermodel spread is about 4 times the IPSL-CM6A-LR intramodel spread: in other words, we can assume that—for atmospheric blocking—the incertitude due to internal variability is considerably smaller than the incertitude due to model properties, putting further attention on each GCM's characteristics.

From what we have seen so far we can robustly state that blocking frequencies have been improved almost everywhere over the Northern Hemisphere from CMIP3 to CMIP6, finding the CMIP5 generation often

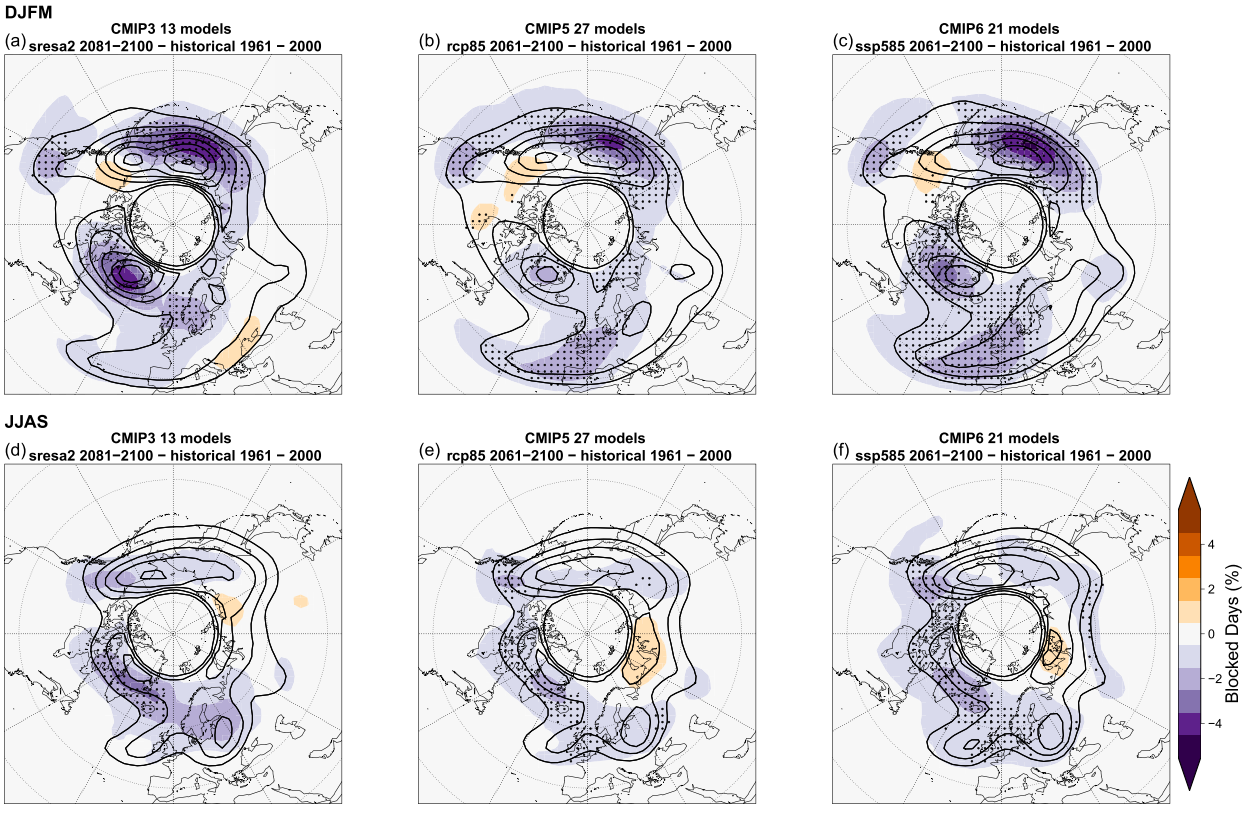

FIG. 6. MMM for blocking frequency in the most extreme climate change scenario (contours) and its difference against the historical period (shading), for (a),(d) CMIP3, (b),(e) CMIP5, and (c),(f) CMIP6 for (top) winter (DJFM) and (bottom) summer (JJAS). Stippling indicates the 5% significance level differences between the MMM of the historical and the MMM of the scenario (with a Welch *t* test). Contours are drawn every 2%. Please note that the color scale is half that in Fig. 1.

as a halfway step. Such improvement can be partially explained with the increased horizontal resolution of the most recent models. However, much more work should be carried out, since the blocking frequency bias over key regions as wintertime central Europe is still large: the CMIP6 MMM still shows about 70% of the OBS blocking frequency, and none of the 31 models analyzed attains the observed frequencies.

4. Climate change scenarios

a. Mean change

The expected impact of greenhouse gases increase on atmospheric blocking frequencies is assessed by Fig. 6, where the differences between the future scenarios climatologies (2061–2100 for RCP8.5 CMIP5 and SSP5–8.5 CMIP6, 2081–2100 for SRES-A2 CMIP3) and the present-day climatologies (1961–2100) are shown. For this analysis, only models where both the historical and the scenario runs are available have been selected: we thus reduced our analysis to 13 CMIP3 models, 27 CMIP5 models, and 21 CMIP6 models.

In winter, the MMM of all CMIP families indicates a decrease in blocking activity (Figs. 6a–c); a significant decrease is found over eastern Siberia and western North America. A slight increase over Alaska and western Canada—associated with westward migration of the blocking maximum following a strengthening and extension of the Pacific jet stream (see Fig. S7)—does not attain the 5% significance level. Over the Atlantic sector, the reduction is observed everywhere, with statistically robust results for all MMMs over western and central Europe. Over Greenland only CMIP6 models show a robust decrease.

Also during the warm season negative signs dominate the changes in blocking frequencies (Figs. 6d–f). However, the signal over the Pacific is less robust, while more agreement among the MMMs is seen over the Greenland sector. Conversely, it is possible to note an increase of blocking frequencies at high latitudes over the Kara Sea in the Ural sector, which is emerging in the three MMMs but never in a statistically significant way.

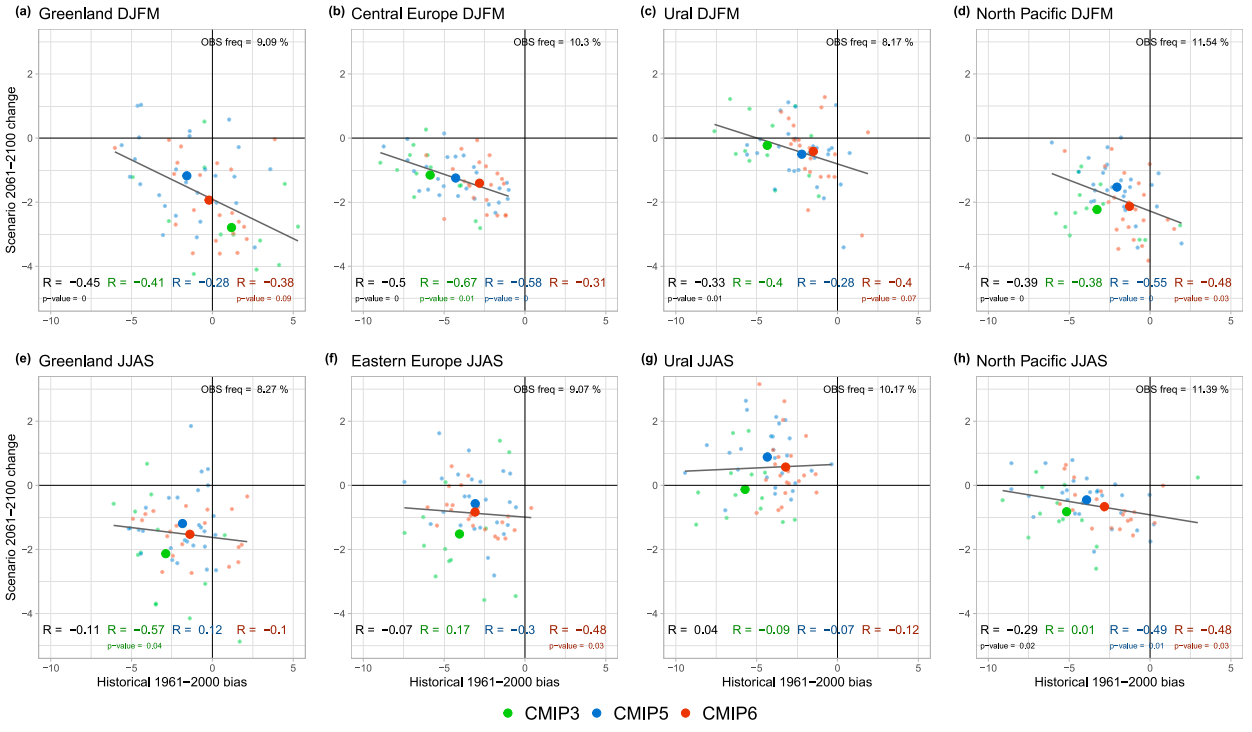

FIG. 7. Scatterplots between the model bias in the historical period and the model-predicted change in the most extreme scenario over the (a),(e) Greenland, (b),(f) central/eastern Europe, (c),(g) Ural, and (d),(h) North Pacific regions for (top) winter (DJFM) and (bottom) summer (JJAS). The gray line represents the linear fit among all the data. The Pearson correlation coefficients and their p values (only when the 10% significance level with a t test is achieved) are shown at the bottom of each panel: black is for the full CMIP dataset, and colors are used for the different intercomparison projects. The observed blocking frequency for the historical period (%, according to the geopotential height index) is shown at the top of each panel.

b. *Relationship with present day*

An interesting emerging feature of winter blocking frequencies across all the CMIP families is the relation between the blocking bias in historical simulations and the blocking changes in the scenario runs.

This is shown by the scatterplots in the top row of Fig. 7 where a negative and statistically significant correlation (at 5% level) is observed (mostly evident over Europe and Greenland with −0.50 and −0.45, respectively). For wintertime blocking such a relationship can be summarized as "the more blocking you have, the larger the blocking decrease will be in the future." At first order, this appears to be reasonable because in order to reduce a phenomenon this has to be simulated: for instance, with an observed frequency over the European sector of 10.3% it is clear that a model that has a bias on the order of −8% would never be able to show a significant decrease (Fig. 7a). However, such behavior is observed also in models with a reasonable bias and over the Greenland, Ural, and North Pacific regions (Figs. 7b–d, where the biases are occasionally positive).

It is thus possible to extrapolate a (tentative) realistic value for the decrease of the blocking frequency over winter central Europe: it should be around −2% (Fig. 7a). Keeping in mind the observed frequency of 10.3%, this means a 1/5 reduction of blocking by the end of the twenty-first century. Indeed, in all winter sectors the linear fit crosses the zero-bias line with negative values of predicted blocking change, suggesting a coherent signal for decreased blocking activity. In other words, also models that have no bias simulate a reduced blocking frequency in the future.

Conversely, during summer the relationship is much less robust (bottom row of Fig. 7), with only North Pacific reaching the 5% significance level.

Figure 7 also shows that the spread among the predicted change can be quite small in some regions, as wintertime central Europe or summertime North Pacific, and quite large in others as summer and winter Greenland and summer eastern Europe. Furthermore, as already mentioned in section 4a, Fig. 7 highlights that for many models the bias is still larger than the climate change signal.

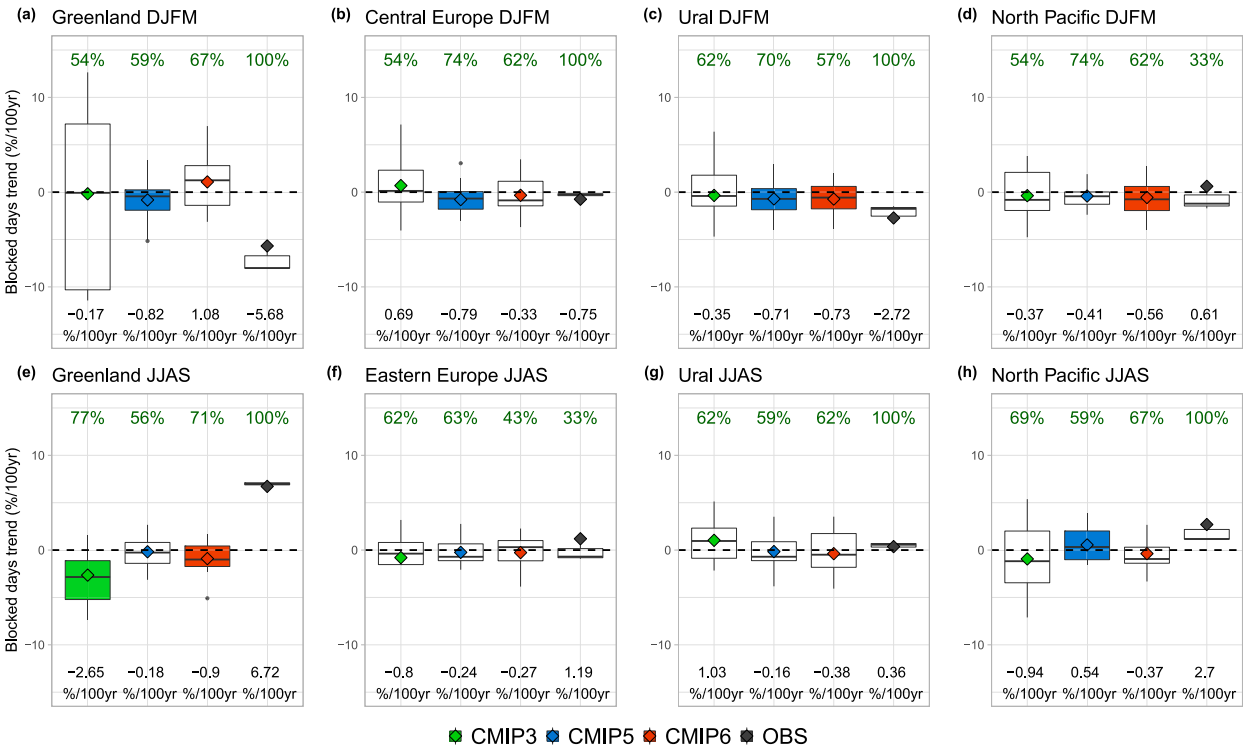

FIG. 8. (a)–(d) DJFM and (e)–(h) JJAS boxplots of the linear trends expressed as percentage of blocked days per 100 years over the 1951–2017 period for the (a),(e) Greenland, (b),(f) central/eastern Europe, (c),(g) Ural, and (d),(h) North Pacific regions. The MMM linear trend (which is different from the mean of the linear trends) is shown by diamonds and reported at the bottom of each panel. The boxplots are colored when the MMM trend significance following a Mann–Kendall test is lower than the 5% level. The model sign agreement (%) is shown in green at the top of each panel. Boxplot properties are as in Fig. 2.

c. *Trends*

The changes in blocking frequencies seen in Fig. 6 are quite evident, but Fig. 7 shows that there is quite a large spread among different models, which oscillates from region to region. Figure 8 explores the robustness of the blocking frequency trends over the observational period (1951–2017): these are obtained by a linear fit to the seasonally averaged blocking frequency. Since the historical simulations end a few years before 2017 (and this is changing in the different CMIP projects), the final years are taken from the scenario runs. The complete time series for the MMMs and their standard deviation are shown for completeness in the Figs. S8 (for winter) and S9 (for summer).

Each panel of Fig. 8 shows the boxplot (i.e., the spread) of the linear trends over a selected region and season. The value of the MMM trend as well as the model sign agreement (i.e., the percentage of models sharing its linear trend with the sign of the MMM is plotted too). Boxplots are filled only when the MMM linear trend attains the 5% significance level with a Mann–Kendall test. Please note that since the MMM trend is different from the mean of each model trend, sometimes the model sign agreement can be lower than 50%. The trends are expressed as the change of the percentage of blocked days per season in 100 years: a value of $+10\%\ (100\,\mathrm{yr})^{-1}$ implies that there is an increase of 10% of blocked days (i.e., about 12 days more for the DJFM season). This means that percentage changes are absolute, not relative.

Figure 8 highlights that the observational records are characterized by an opposite behavior between summer and winter: linear trends are negative in winter and positive for summer. Given the large interannual variability of blocking, most trends are not significant. Only over the summer Greenland sector the 5% significance level to a Mann–Kendall test is achieved, showing a marked increase in blocking activity $[+6.72\%\ (100\,\mathrm{yr})^{-1}]$ as also reported in the literature (Hanna et al. 2016).

CMIP runs, conversely, show both decreasing and increasing trends, with weak agreement inside each comparison project and among the project themselves (which can be seen by the large distance among the whiskers, especially over Greenland). The 95% confidence level is attained in a few instances, and the sign agreement is often around 60% (meaning that 2/5 of the

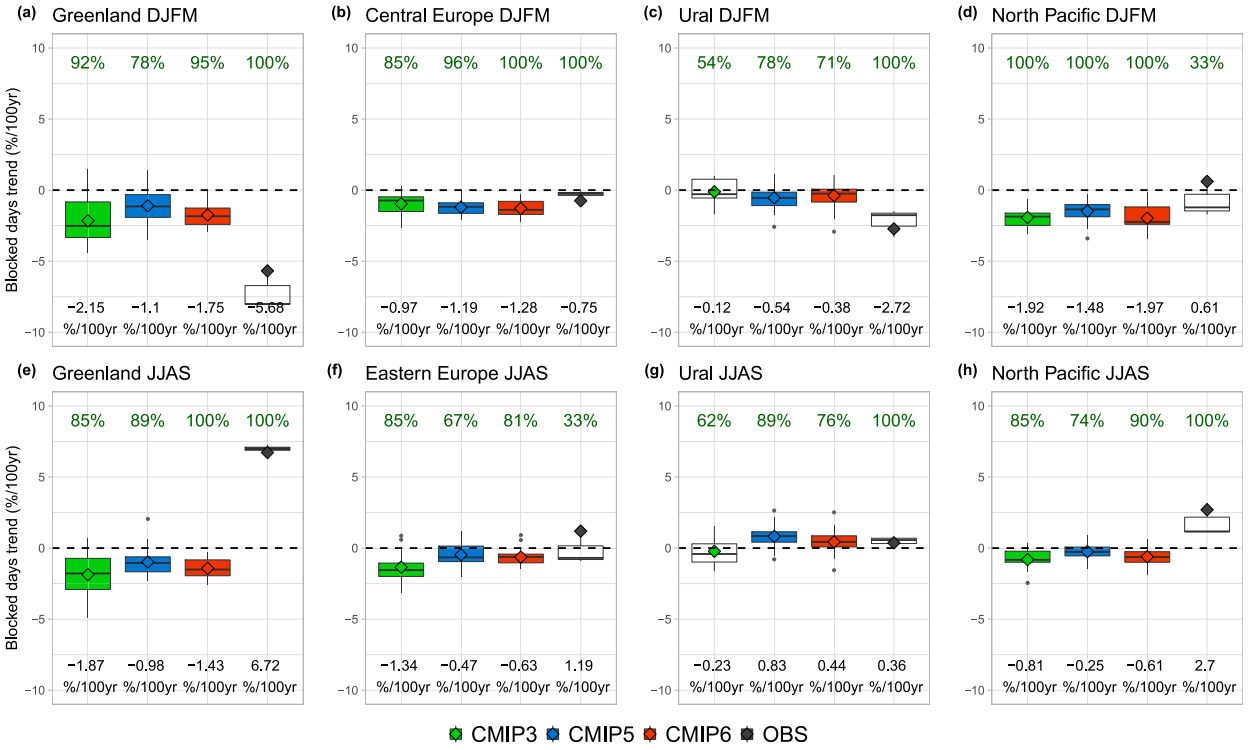

FIG. 9. As in Fig. 8, but across the whole period available (1951–2100).

models show an opposite trend). The only exception is the behavior of the CMIP5 MMM during winter, which shows significant negative trends with larger model sign agreement (around 70%) in the Greenland, Europe, and Ural sectors.

The situation changes radically when the analysis is extended to the whole time window available (1951–2100). This is shown in Fig. 9. For almost all the regions and for all the CMIP families the MMMs show a remarkable negative trend that is significant at the 5% significance level with a Mann–Kendall test. This is reinforced by the fact that the sign agreement is reaching in many cases 100%, meaning that all models have trends with the same negative sign. Trends are larger in winter (Figs. 9a–d), when they are about -1.5% $(100\,\mathrm{yr})^{-1}$, and smaller in summer, when they hardly reach -1% $(100\,\mathrm{yr})^{-1}$ (Figs. 9e–g). The only exception is again the summer Ural sector, where both CMIP5 and CMIP6 show a significant positive trend (Fig. 9h).

All the above-mentioned findings can be questioned considering the limited agreement of models with OBS, especially for the warm season. For example, summer Greenland blocking already shows significant disagreement between the observation and the CMIP models over the historical period [which has been noticed also by Hanna et al. (2018) for CMIP5 models]. However, the limited length of the observational dataset and the fact that the largest increase in global surface temperature is expected to occur in the scenarios must be kept in mind when comparing OBS and CMIP models, especially over the full time window (1951–2100). One possibility is thus that the agreement among models and reanalyses will emerge more clearly in the next decades. Assuming the modeled trends are correct, and that the variability of blocking is equally well simulated, we can speculate that the signal of observed change of blocking will emerge from noise at a certain moment in the future. The time series have been analyzed in order to detect the first year for each sector for which the Mann–Kendall test achieves (and maintains in the following years) the 5% significance level: we will call it the signal-emerging year. If the signal-emerging year is far in the future, the disagreement between OBS and model is somewhat less worrying. The results are reported in Table 2.

On average, the signal-emerging year is occurring around the half of the twenty-first century (2040–60). It is occurring before in winter than in summer and CMIP5 models tend to show sooner emerging years than CMIP6 models.

More generally, summer and winter trends suggest different conclusions. In winter, all CMIPs find

TABLE 2. Signal-emerging year (i.e., the first year for which the Mann–Kendall test on the linear trend in the MMM blocking frequency achieves the 5% significance level; see text for details) for the different blocking sectors and seasons. Arrows show the sign of the trend. Since CMIP3 data are not continuous in time, they are not included in this analysis.

Season	Sector	OBS	CMIP5	CMIP6
DJFM	Greenland	—	↓ 2022	↓ 2054
	Central Europe	—	↓ 2008	↓ 2029
	Ural	—	↓ 2002	↓ 2055
	North Pacific	—	↓ 2024	↓ 2025
JJAS	Greenland	↑ 1992	↓ 2033	↓ 2046
	Eastern Europe	—	↓ 2054	↓ 2062
	Ural	—	↑ 2050	↑ 2093
	North Pacific	—	↓ 2095	↓ 2038

significant negative trends that will emerge as statistically significant only in the future (for CMIP6 the first one is winter North Pacific in 2025), while the same negative trends of OBS are not significant. This could mean that the signal from such decreasing trend will be emerging from natural variability–induced noise in the next years also in observations. However, the fact that CMIP5 models detect significant trends starting from the early decades of 2000 brings into question the reliability of CMIP5 future scenarios also in winter. In summer, in order to have agreement between modeled and observed trends, one should hope that a reversal of the trends sign of the observation happens in the future. This is unlikely to happen if the signal-emerging year is close in the future, as is the case for Greenland (e.g., 2033 in CMIP5 and 2046 in CMIP6).

It is fair to conclude that whereas reasonable confidence should be attributed to modeled trends for winter blocking frequency, the confidence for summer blocking must be low.

d. Interannual variability

Blocking is characterized by large natural variability (Davini et al. 2012), which can often lead to a year with large blocking frequency followed by a year with no blocking at all. Figure 10 compares the boxplots of the interannual variability in historical (1961–2000) and scenario (2061–2100) simulations over the four different summer and winter regions. Here, the interannual variability of each model is measured as the standard deviation of its seasonally averaged time series.

CMIP models are characterized by large spread (defined by the extension of the boxplot), but overall they tend to underestimate the interannual variability when compared to OBS. A exception is the summertime Greenland blocking (Fig. 10e), where the variability is about 20% larger than observed. This, and the previous finding about the trend (Fig. 9), point to the fact that the models are struggling in correctly representing the dynamical mechanisms that govern Greenland blocking during summer. The Greenland sector is also problematic for the cold season (Fig. 10b). Here CMIP5 and CMIP6 underestimate the interannual variability by 30%, and the spread of the models is very large, underlining the disagreement among the models.

Figures 10a–d also tell us that in winter the interannual variability is expected to decrease at the end of the twenty-first century, with the purple bars always lower than the green bars. However, due to the large spread, the 5% statistical significance level is never achieved.

Conversely, nothing clear is detectable in summer, suggesting that even with fewer blocking events (as seen in Fig. 6) the interannual variability may remain similar as today. A clear exception is the Ural sector where the interannual variability is expected to increase, putting further attention on this region where positive trends have been detected.

5. Sensitivity to global temperature changes

CMIP models are characterized by a large spread in the expected global surface temperature change at the end of twenty-first century, ranging from 2.5°C up to almost 6°C (not shown). The ''climate sensitivity of atmospheric blocking'' (i.e., the response of blocking to a given level of global warming) could be then potentially very different in each model and in each region of the globe. It should be also noticed that the different intercomparison projects show a wide spectrum of different temperature changes at the end of the century, with CMIP6 showing larger increases (see Table 1). To reduce the noise as much as possible, all the models belonging to the three different intercomparison projects are analyzed as a single ensemble. Only four models (CMIP5 BNU-ESM and CMIP6 GFDL-CM4, MPI-ESM1-2-HR, and HadGEM3-GC31-MM) have been excluded due to unavailability of 2-m temperature data. A measure of the response of blocking to global warming is then estimated linearly regressing in the model space the blocking frequency changes (differences between the scenario and the historical period) against the globally averaged 2-m temperature change over the same period: the results are shown in Fig. 11. Blue color points to regions where a larger global warming favors a stronger reduction of blocking frequency, red colors show areas where warmer global mean temperature lead to an increase of blocking.

Interestingly, only three blocking regions seem to be directly related to the amount of warming at a statistically significant level. Of course, these are the regions

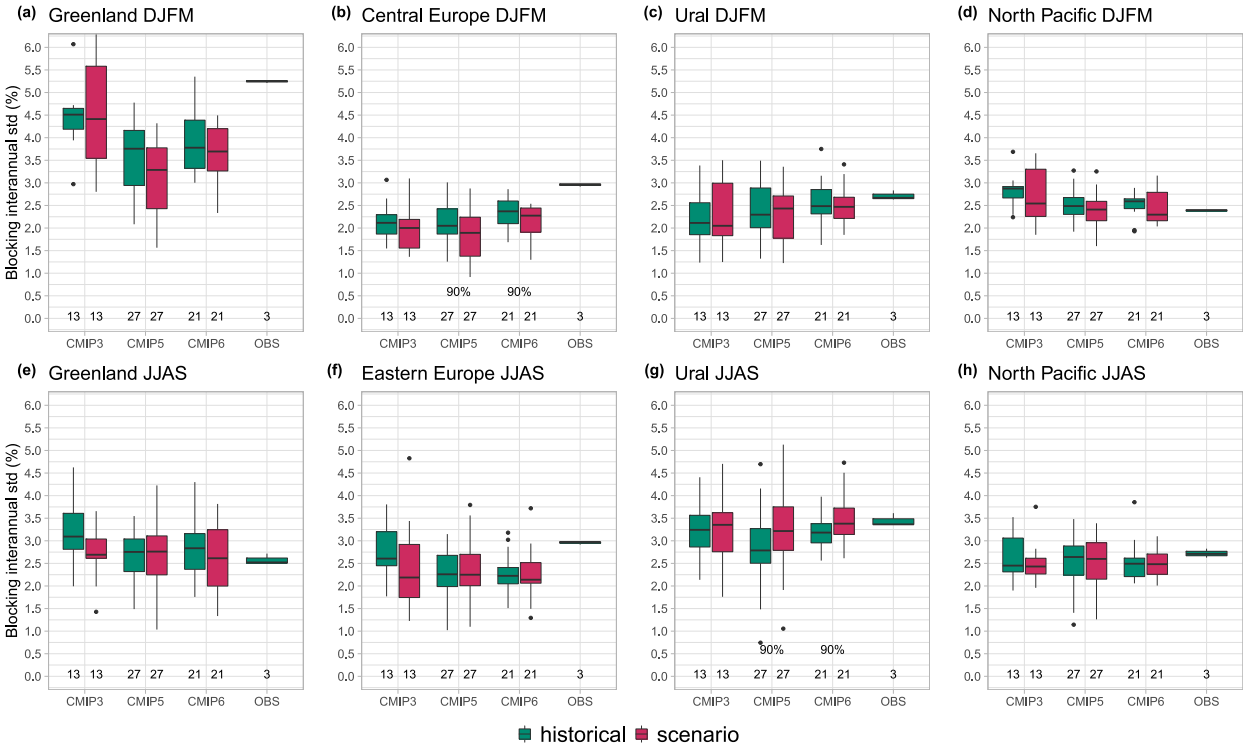

FIG. 10. Boxplots showing blocking frequency interannual standard deviation over the (a),(e) Greenland, (b),(f) central/eastern Europe, (c),(g) Ural, and (d),(h) North Pacific regions in the historical (1961–2000) and scenario (2061–2100) period for (top) winter (DJFM) and (bottom) summer (JJAS). When lower than the 10% level (with a Welch *t* test), statistically significant differences between historical and future period are shown at the bottom of each panel. The number of models included in each bar is reported at the bottom of each panel. Boxplot properties are as in Fig. 2.

where the linear regressions on CMIP3, CMIP5, and CMIP6 agree among each other (Fig. S10). In winter a larger climate sensitivity suggests a stronger decrease of blocking over the European and the North Pacific sector, whereas in summer a stronger climate sensitivity points to an increase in blocking frequency over the Urals.

In all other regions trends are detected but they are not significant, suggesting for example, that Greenland

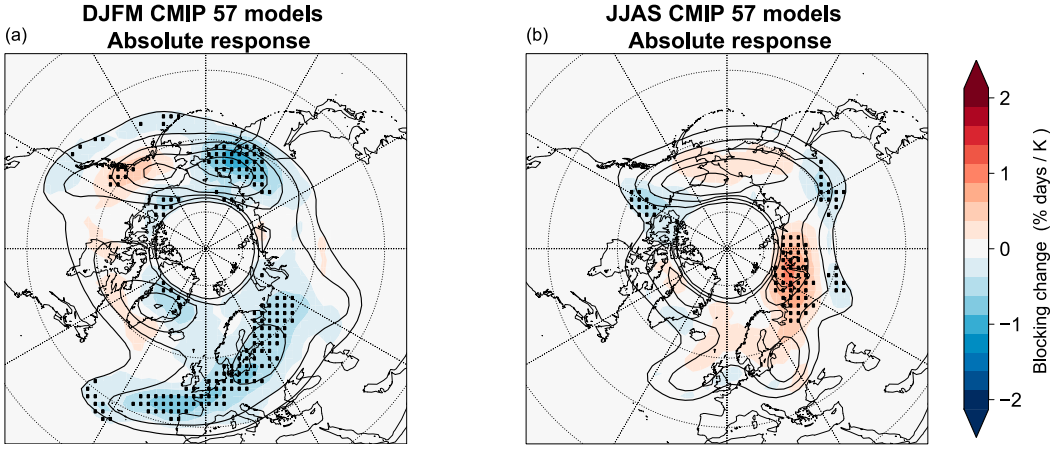

FIG. 11. (a) DJFM and (b) JJAS linear regression between the blocking frequency response and the global mean temperature response across the totality of CMIP models (shading) and the blocking frequency in the 2061–2100 scenario (contours). Contours are drawn every 2%. Regression coefficients are plotted only for blocking frequency greater than 2%. Stippling shows coefficients significant at the 5% level with a *t* test.

blocking intermodel variability could not be explained simply by global warming itself. It is therefore possible that other more regional phenomena, such as the tropical or the polar amplification as well as specific SST patterns (Matsueda and Endo 2017), have a stronger impact on the blocking activity. The relationship between these or other climate "remote drivers" (Manzini et al. 2014) and atmospheric blocking changes is beyond the goal of the current analysis, and will be the subject of a forthcoming study.

6. Discussion and conclusions

Winter and summer Northern Hemisphere atmospheric blocking has been analyzed in three different intercomparison projects that encompass 12 years of climate model development. Data from CMIP3 (2007), CMIP5 (2012), and CMIP6 (2019) have been analyzed, and compared against three different reanalysis datasets (NCEP–NCAR, JRA-55, and ERA-40/ERA-Interim). This huge dataset made by more than 75 models provided the material for a deep investigation of the ability of GCMs in reproducing atmospheric blocking in the present-day climate and in estimating it in the future scenarios.

Overall, blocking can be described as an ongoing but successful great challenge for the climate modeling community. Although the most recent generation of models (i.e., CMIP6) still show significant bias in blocking frequency in key regions as the European winter, the effort by modelers has led to large improvements, which—on average—have halved the biases that were usual for models of 12 years ago. This has been certainly made possible by larger availability of computational power, since horizontal resolution moved from about 4° in CMIP3 models up to 2.2° in CMIP6 models (see Table 1). Indeed, grid refinement has been shown to be one of the reasons able to explain the observed improvement. Positive but less confident benefits could come also from the reduction of the North Atlantic and North Pacific SST bias. The ensemble spread is also slightly reduced in CMIP6 when compared to CMIP5, suggesting a larger agreement among the different models.

Results are not equally good for the future climate trends. A distinction must be made between summer and winter; in winter, the vast majority of models points to a worldwide reduction of the blocking activity that seems to be found—although not in a statistically significant way—in current observed trends. Interestingly, models that show larger blocking frequencies (i.e., smaller bias) in present-day simulations are often associated with a larger decrease in the future, which adds credibility to the robustness of the observed decrease.

The situation is more complex for summertime blocking. Observations show an increase of blocking activity, strong and significant over Greenland: this increasing trend is not captured at all by CMIP models. On the contrary, most models project a decrease of blocking activity. An interesting exception is the summer Ural blocking: here, while observations point to a decrease, CMIP5 and CMIP6 models suggest an increase of blocking frequency possibly bound to emerge from noise in the second half of the twenty-first century. Considering these contradictory results in terms of trends and the fact that biases of the CMIP models are, on average, at least twice the climate change signals, we conclude that we should not be very confident with summer atmospheric blocking future prediction.

Blocking duration deserves a special comment. As mentioned in section 2, the current analysis has been carried out without taking into consideration any spatial and temporal filters, so that blocking duration has not been directly analyzed. However, in Figs S5 and S6 the differences between future and historical blocking events frequency applying a 5- and 10-day filtering are shown. Overall, patterns and trends reflect what shown by Fig. 6 although smaller areas of significant signal are detected as long as the temporal filtering is increased (following the reduction of the number of blocking events examined). It is however interesting to notice that summer Ural blocking emerges as clearly increasing, especially when the 10-day filter is applied. This result suggests that long-lasting Ural blocking events could be increasing, which may have a remarkable impact on the local weather. This can have implications for 1) extreme events for the next century over western Russia and eastern Europe, considering the connection between summer blocking and heat waves in this region (Barriopedro et al. 2011; Schaller et al. 2018), and in 2) the framework of Arctic climate change since ice depletion in the Barents–Kara Seas has been connected with Ural blocking (Gong and Luo 2017; Tyrlis et al. 2019).

In the last part of the work we have also investigated the relationship between global warming and blocking, which is particularly interesting since CMIP6 models show a larger climate sensitivity and a larger spread in its estimate compared to their predecessors (see Table 1, or, e.g., Gettelman et al. 2019). We found that a larger warming would be accompanied by a stronger decrease of blocking activity over Europe and North Pacific in the winter season, whereas it would lead to a more evident increase over the Ural sector during summertime.

To conclude, in order to reconcile the present work with the previous findings of Davini and D'Andrea (2016), which analyzed the biases of an older set of

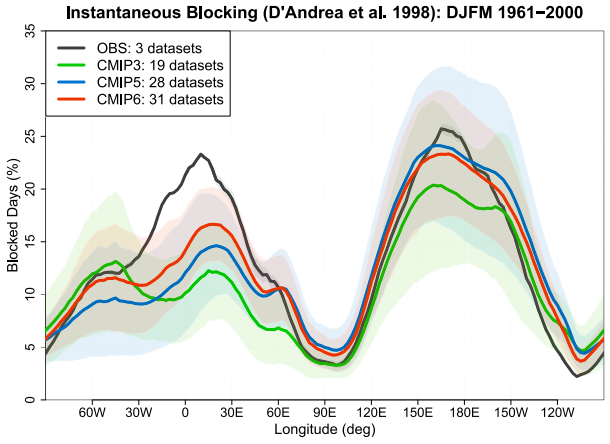

FIG. 12. DJFM 1961–2010 instantaneous blocking frequency according to the D'Andrea et al. (1998) index. MMM is shown by the bold line; shading shows the ensemble standard deviation.

model generation over a shorter time window (1979–88 DJF), Fig. 12 replicates their Fig. 3, showing the MMM of the instantaneous blocking frequency for the D'Andrea et al. (1998) one-dimensional index. A few minor differences are however necessary: the index is here adapted for a 2.5° × 2.5° grid and the period of analysis is extended to the 1961–2000 DJFM season. Although 1D indices provide a picture of the atmospheric blocking biases with a slightly different flavor than 2D indices, Fig. 12 illustrates that the findings of the present work largely agree with what Davini and D'Andrea (2016) reported. North Pacific biases are small compared to long-lasting Euro-Atlantic bias, which however has been alleviated moving from CMIP3 to CMIP5 up to CMIP6.

Although the improvements are easily seen, there are a few things on which blocking research with GCMs should be focused:

1) European blocking biases are still large, and often larger than the climate change signal. The benefit of increasing resolution would probably be unable to bring a further step up in blocking representation, so more detailed analysis on physical processes influencing blocking is in order. For instance, studies investigating the effect in GCM of the orography representation (Pithan et al. 2016) or of diabatic heating in the extratropics (Pfahl et al. 2015) should be pursued.
2) Present-day observational trends disagree with climate models results, especially in summer and over Greenland. It is a red alert for climate modelers since it could point to a fundamental deficiency in the dynamical representation of blocking—and more generally midlatitude climate—and its response to climate change. This may also bring into question the trends in the winter season.
3) Although blocking will generally be decreasing in the future, hence reducing its impacts in many parts of the globe, CMIP models suggest that some regions would face an increase of blocking activity. Summer Ural blocking could be affected by these changes, being particularly sensitive to global temperature increase and to long-lasting blocking events. Considering the expected warmer surface temperatures, this has the worrying potential for severe impact on human activities. More detailed analysis should be carried out in this direction.

Acknowledgments. The authors want to thank all modeling groups participating in CMIP3, CMIP5, and CMIP6 for producing and sharing model data. The JPI-Climate/Belmont Forum project GOTHAM (ANR-15-JCLI-0004-01) partly supported the work. Paolo Davini acknowledges support by the PRIMAVERA project, funded by the European Commission under grant agreement 641727 of the Horizon 2020 research program.

REFERENCES

Anstey, J. A., and Coauthors, 2013: Multi-model analysis of Northern Hemisphere winter blocking: Model biases and the role of resolution. *J. Geophys. Res. Atmos.*, **118**, 3956–3971, https://doi.org/10.1002/jgrd.50231.

Barnes, E. A., and D. Hartmann, 2010: Influence of eddy-driven jet latitude on North Atlantic jet persistence and blocking frequency in CMIP3 integrations. *Geophys. Res. Lett.*, **37**, L23802, https://doi.org/10.1029/2010gl045700.

——, J. Slingo, and T. Woollings, 2012: A methodology for the comparison of blocking climatologies across indices, models and climate scenarios. *Climate Dyn.*, **38**, 2467–2481, https://doi.org/10.1007/s00382-011-1243-6.

——, E. Dunn-Sigouin, G. Masato, and T. Woollings, 2014: Exploring recent trends in Northern Hemisphere blocking. *Geophys. Res. Lett.*, **41**, 638–644, https://doi.org/10.1002/2013GL058745.

Barriopedro, D., R. Garcia-Herrera, and R. Trigo, 2010: Application of blocking diagnosis methods to general circulation models. Part I: A novel detection scheme. *Climate Dyn.*, **35**, 1373–1391, https://doi.org/10.1007/s00382-010-0767-5.

——, E. M. Fischer, J. Luterbacher, R. M. Trigo, and R. García-Herrera, 2011: The hot summer of 2010: Redrawing the temperature record map of Europe. *Science*, **332**, 220–224, https://doi.org/10.1126/science.1201224.

Berrisford, P., B. Hoskins, and E. Tyrlis, 2007: Blocking and Rossby wave breaking on the dynamical tropopause in the Southern Hemisphere. *J. Atmos. Sci.*, **64**, 2881–2898, https://doi.org/10.1175/JAS3984.1.

Cheung, H. N., W. Zhou, Y. Shao, W. Chen, H. Y. Mok, and M. C. Wu, 2013: Observational climatology and characteristics of wintertime atmospheric blocking over Ural–Siberia. *Climate Dyn.*, **41**, 63–79, https://doi.org/10.1007/s00382-012-1587-6.

D'Andrea, F., and Coauthors, 1998: Northern Hemisphere atmospheric blocking as simulated by 15 atmospheric general cir-

culation models in the period 1979–1988. *Climate Dyn.*, **14**, 385–407, https://doi.org/10.1007/s003820050230.

Davini, P., 2019: MiLES—Mid-Latitude Evaluation System. GitHub, https://github.com/oloapinivad/MiLES.

——, and F. D'Andrea, 2016: Northern Hemisphere atmospheric blocking representation in global climate models: Twenty years of improvements? *J. Climate*, **29**, 8823–8840, https://doi.org/10.1175/JCLI-D-16-0242.1.

——, C. Cagnazzo, S. Gualdi, and A. Navarra, 2012: Bidimensional diagnostics, variability and trends of Northern Hemisphere blocking. *J. Climate*, **25**, 6496–6509, https://doi.org/10.1175/JCLI-D-12-00032.1.

——, S. Corti, F. D'Andrea, G. Rivière, and J. von Hardenberg, 2017: Improved winter European atmospheric blocking frequencies in high-resolution global climate simulations. *J. Adv. Model. Earth Syst.*, **9**, 2615–2634, https://doi.org/10.1002/2017MS001082.

Dee, D., and Coauthors, 2011: The ERA-Interim reanalysis: Configuration and performance of the data assimilation system. *Quart. J. Roy. Meteor. Soc.*, **137**, 553–597, https://doi.org/10.1002/qj.828.

Delcambre, S. C., D. J. Lorenz, D. J. Vimont, and J. E. Martin, 2013: Diagnosing Northern Hemisphere jet portrayal in 17 CMIP3 global climate models: Twenty-first-century projections. *J. Climate*, **26**, 4930–4946, https://doi.org/10.1175/JCLI-D-12-00359.1.

Dole, R., and N. Gordon, 1983: Persistent anomalies of the extratropical Northern Hemisphere wintertime circulation: Geographical distribution and regional persistence characteristics. *Mon. Wea. Rev.*, **111**, 1567–1586, https://doi.org/10.1175/1520-0493(1983)111<1567:PAOTEN>2.0.CO;2.

Dunn-Sigouin, E., and S.-W. Son, 2013: Northern Hemisphere blocking frequency and duration in the CMIP5 models. *J. Geophys. Res. Atmos.*, **118**, 1179–1188, https://doi.org/10.1002/jgrd.50143.

Dunstone, N., D. Smith, A. Scaife, L. Hermanson, R. Eade, N. Robinson, M. Andrews, and J. Knight, 2016: Skilful predictions of the winter North Atlantic Oscillation one year ahead. *Nat. Geosci.*, **9**, 809–814, https://doi.org/10.1038/ngeo2824.

Eyring, V., S. Bony, G. A. Meehl, C. A. Senior, B. Stevens, R. J. Stouffer, and K. E. Taylor, 2016: Overview of the Coupled Model Intercomparison Project phase 6 (CMIP6) experimental design and organization. *Geosci. Model Dev.*, **9**, 1937–1958, https://doi.org/10.5194/gmd-9-1937-2016.

Francis, J. A., and S. J. Vavrus, 2012: Evidence linking Arctic amplification to extreme weather in mid-latitudes. *Geophys. Res. Lett.*, **39**, L06801, https://doi.org/10.1029/2012GL051000.

Gettelman, A., and Coauthors, 2019: High climate sensitivity in the Community Earth System Model version 2 (CESM2). *Geophys. Res. Lett.*, **46**, 8329–8337, https://doi.org/10.1029/2019GL083978.

Gollan, G., S. Bastin, and R. J. Greatbatch, 2019: Tropical precipitation influencing boreal winter midlatitude blocking. *Atmos. Sci. Lett.*, **20**, e900, https://doi.org/10.1002/asl.900.

Gong, T., and D. Luo, 2017: Ural blocking as an amplifier of the Arctic sea ice decline in winter. *J. Climate*, **30**, 2639–2654, https://doi.org/10.1175/JCLI-D-16-0548.1.

Hanna, E., T. E. Cropper, R. J. Hall, and J. Cappelen, 2016: Greenland blocking index 1851–2015: A regional climate change signal. *Int. J. Climatol.*, **36**, 4847–4861, https://doi.org/10.1002/joc.4673.

——, X. Fettweis, and R. J. Hall, 2018: Brief communication: Recent changes in summer Greenland blocking captured by none of the CMIP5 models. *Cryosphere*, **12**, 3287–3292, https://doi.org/10.5194/tc-12-3287-2018.

Hinton, T., B. Hoskins, and G. Martin, 2009: The influence of tropical sea surface temperatures and precipitation on North Pacific atmospheric blocking. *Climate Dyn.*, **33**, 549–563, https://doi.org/10.1007/s00382-009-0542-7.

Jung, T., and Coauthors, 2010: The ECMWF model climate: Recent progress through improved physical parametrizations. *Quart. J. Roy. Meteor. Soc.*, **136**, 1145–1160, https://doi.org/10.1002/qj.634.

——, and Coauthors, 2012: High-resolution global climate simulations with the ECMWF model in Project Athena: Experimental design, model climate, and seasonal forecast skill. *J. Climate*, **25**, 3155–3172, https://doi.org/10.1175/JCLI-D-11-00265.1.

Kalnay, E., and Coauthors, 1996: The NCEP/NCAR 40-Year Reanalysis Project. *Bull. Amer. Meteor. Soc.*, **77**, 437–471, https://doi.org/10.1175/1520-0477(1996)077<0437:TNYRP>2.0.CO;2.

Kobayashi, S., and Coauthors, 2015: The JRA-55 reanalysis: General specifications and basic characteristics. *J. Meteor. Soc. Japan*, **93**, 5–48, https://doi.org/10.2151/jmsj.2015-001.

Luo, D., Y. Xiao, Y. Yao, A. Dai, I. Simmonds, and C. L. Franzke, 2016: Impact of Ural blocking on winter warm Arctic–cold Eurasian anomalies. Part I: Blocking-induced amplification. *J. Climate*, **29**, 3925–3947, https://doi.org/10.1175/JCLI-D-15-0611.1.

Manzini, E., and Coauthors, 2014: Northern winter climate change: Assessment of uncertainty in CMIP5 projections related to stratosphere–troposphere coupling. *J. Geophys. Res. Atmos.*, **119**, 7979–7998, https://doi.org/10.1002/2013jd021403.

Masato, G., B. J. Hoskins, and T. Woollings, 2013: Winter and summer Northern Hemisphere blocking in CMIP5 models. *J. Climate*, **26**, 7044–7059, https://doi.org/10.1175/JCLI-D-12-00466.1.

Matsueda, M., and H. Endo, 2017: The robustness of future changes in Northern Hemisphere blocking: A large ensemble projection with multiple sea surface temperature patterns. *Geophys. Res. Lett.*, **44**, 5158–5166, https://doi.org/10.1002/2017GL073336.

——, R. Mizuta, and S. Kusunoki, 2009: Future change in wintertime atmospheric blocking simulated using a 20-km-mesh atmospheric global circulation model. *J. Geophy. Res.*, **114**, D12114, https://doi.org/10.1029/2009JD011919.

Meehl, G. A., C. Covey, K. E. Taylor, T. Delworth, R. J. Stouffer, M. Latif, B. McAvaney, and J. F. Mitchell, 2007: The WCRP CMIP3 multimodel dataset: A new era in climate change research. *Bull. Amer. Meteor. Soc.*, **88**, 1383–1394, https://doi.org/10.1175/BAMS-88-9-1383.

Moss, R., and Coauthors, 2010: The next generation of scenarios for climate change research and assessment. *Nature*, **463**, 747–756, https://doi.org/10.1038/nature08823.

Nakicenovic, N., and Coauthors, 2000: IPCC Special Report on Emissions Scenarios (SRES). Cambridge University Press, 599 pp.

O'Neill, B. C., and Coauthors, 2016: The Scenario Model Intercomparison Project (ScenarioMIP) for CMIP6. *Geosci. Model Dev.*, **9**, 3461–3482, https://doi.org/10.5194/gmd-9-3461-2016.

O'Reilly, C. H., S. Minobe, and A. Kuwano-Yoshida, 2016: The influence of the Gulf Stream on wintertime European blocking. *Climate Dyn.*, **47**, 1545–1567, https://doi.org/10.1007/s00382-015-2919-0.

Overland, J. E., and Coauthors, 2016: Nonlinear response of mid-latitude weather to the changing Arctic. *Nat. Climate Change*, **6**, 992–999, https://doi.org/10.1038/nclimate3121.

Pelly, J., and B. Hoskins, 2003: A new perspective on blocking. *J. Atmos. Sci.*, **60**, 743–755, https://doi.org/10.1175/1520-0469(2003)060<0743:ANPOB>2.0.CO;2.

Pfahl, S., C. Schwierz, M. Croci-Maspoli, C. M. Grams, and H. Wernli, 2015: Importance of latent heat release in ascending air streams for atmospheric blocking. *Nat. Geosci.*, **8**, 610–614, https://doi.org/10.1038/ngeo2487.

Pinheiro, M. C., P. Ullrich, and R. Grotjahn, 2019: Atmospheric blocking and intercomparison of objective detection methods: Flow field characteristics. *Climate Dyn.*, **53**, 4189–4216, https://doi.org/10.1007/s00382-019-04782-5.

Pithan, F., T. G. Shepherd, G. Zappa, and I. Sandu, 2016: Climate model biases in jet streams, blocking and storm tracks resulting from missing orographic drag. *Geophys. Res. Lett.*, **43**, 7231–7240, https://doi.org/10.1002/2016GL069551.

Prodhomme, C., L. Batté, F. Massonnet, P. Davini, O. Bellprat, V. Guemas, and F. Doblas-Reyes, 2016: Benefits of increasing the model resolution for the seasonal forecast quality in EC-Earth. *J. Climate*, **29**, 9141–9162, https://doi.org/10.1175/JCLI-D-16-0117.1.

Rex, D., 1950: Blocking action in the middle troposphere and its effect upon regional climate: I. An aerological study of blocking action. *Tellus*, **2**, 196–211, https://doi.org/10.3402/tellusa.v2i3.8546.

Scaife, A., T. Woollings, J. Knight, G. Martin, and T. Hinton, 2010: Atmospheric blocking and mean biases in climate models. *J. Climate*, **23**, 6143–6152, https://doi.org/10.1175/2010JCLI3728.1.

——, and Coauthors, 2011: Improved Atlantic winter blocking in a climate model. *Geophys. Res. Lett.*, **38**, L23703, https://doi.org/10.1029/2011GL049573.

Schaller, N., J. Sillmann, J. Anstey, E. M. Fischer, C. M. Grams, and S. Russo, 2018: Influence of blocking on northern European and western Russian heatwaves in large climate model ensembles. *Environ. Res. Lett.*, **13**, 054015, https://doi.org/10.1088/1748-9326/aaba55.

Scherrer, S., M. Croci-Maspoli, C. Schwierz, and C. Appenzeller, 2006: Two-dimensional indices of atmospheric blocking and their statistical relationship with winter climate patterns in the Euro-Atlantic region. *Int. J. Climatol.*, **26**, 233–249, https://doi.org/10.1002/joc.1250.

Schiemann, R., and Coauthors, 2017: The resolution sensitivity of Northern Hemisphere blocking in four 25-km atmospheric global circulation models. *J. Climate*, **30**, 337–358, https://doi.org/10.1175/JCLI-D-16-0100.1.

——, and Coauthors, 2020: Northern Hemisphere blocking simulation in current climate models: Evaluating progress from the climate model intercomparison project phase 5 to 6 and sensitivity to resolution. *Wea. Climate Dyn.*, **1**, 277–292, https://doi.org/10.5194/wcd-1-277-2020.

Schwierz, C., M. Croci-Maspoli, and H. Davies, 2004: Perspicacious indicators of atmospheric blocking. *Geophys. Res. Lett.*, **31**, L06125, https://doi.org/10.1029/2003gl019341.

Sillmann, J., M. Croci-Maspoli, M. Kallache, and R. W. Katz, 2011: Extreme cold winter temperatures in Europe under the influence of North Atlantic atmospheric blocking. *J. Climate*, **24**, 5899–5913, https://doi.org/10.1175/2011JCLI4075.1.

Steinfeld, D., and S. Pfahl, 2019: The role of latent heating in atmospheric blocking dynamics: A global climatology. *Climate Dyn.*, **53**, 6159–6180, https://doi.org/10.1007/s00382-019-04919-6.

——, M. Boettcher, R. Forbes, and S. Pfahl, 2020: The sensitivity of atmospheric blocking to changes in upstream latent heating–numerical experiments. *Wea. Climate Dyn. Discuss.*, https://doi.org/10.5194/wcd-2020-5.

Taylor, K., R. Stouffer, and G. Meehl, 2012: An overview of CMIP5 and the experiment design. *Bull. Amer. Meteor. Soc.*, **93**, 485–498, https://doi.org/10.1175/BAMS-D-11-00094.1.

Tibaldi, S., and F. Molteni, 1990: On the operational predictability of blocking. *Tellus*, **42A**, 343–365, https://doi.org/10.3402/tellusa.v42i3.11882.

Tyrlis, E., E. Manzini, J. Bader, J. Ukita, H. Nakamura, and D. Matei, 2019: Ural blocking driving extreme Arctic sea ice loss, cold Eurasia, and stratospheric vortex weakening in autumn and early winter 2016–2017. *J. Geophys. Res. Atmos.*, **124**, 11 313–11 329, https://doi.org/10.1029/2019jd031085.

Uppala, S. M., and Coauthors, 2005: The ERA-40 Re-Analysis. *Quart. J. Roy. Meteor. Soc.*, **131**, 2961–3012, https://doi.org/10.1256/qj.04.176.

Woollings, T., A. Hannachi, B. Hoskins, and A. Turner, 2010: A regime view of the North Atlantic Oscillation and its response to anthropogenic forcing. *J. Climate*, **23**, 1291–1307, https://doi.org/10.1175/2009JCLI3087.1.

——, and Coauthors, 2018: Blocking and its response to climate change. *Curr. Climate Change Rep.*, **4**, 287–300, https://doi.org/10.1007/s40641-018-0108-z.